Hydrology and Earth System Sciences Discussions

HESSD

6, 4813–4861, 2009

WGHM calibration analysis with GRACE

S. Werth and A. Güntner

Title Page	
Abstract	Introduction
Conclusions	References
Tables	Figures
◄◄	►►
◄	►
Back	Close
Full Screen / Esc	
Printer-friendly Version	
Interactive Discussion	

Calibration analysis for water storage variability of the global hydrological model WGHM

S. Werth and A. Güntner

Deutsches GeoForschungsZentrum GFZ, Telegrafenberg, 14473 Potsdam, Germany

Correspondence to: S. Werth (swerth@gfz-potsdam.de)

Abstract

This study contributes to an improved global simulation of continental water storage variations by calibrating the WaterGAP Global Hydrology Model (WGHM) for 28 of the largest river basins worldwide. Five years (01/2003–12/2007) of satellite-based estimates of total water storage changes from the GRACE mission are combined with river discharge data in a multi-objective calibration framework of the most sensitive WGHM model parameters. The uncertainty and significance of the calibration results is analyzed with respect to errors in the observation data. An independent simulation period (01/2008–12/2008) is used for validation. The contribution of single storage compartments to the total water budget before and after calibration is analyzed in detail. A multi-objective improvement of the model states is obtained for most of the river basins, with mean error reductions up to 110 km^3/month for discharge and up to 24 mm of a water mass equivalent column for total water storage changes, as for the Amazon basin. Errors in phase and signal variability of seasonal water mass changes are reduced. The calibration is shown to primarily affect soil water storage in most river basins. The variability of groundwater storage variations is reduced at the global scale after calibration. Structural model errors are identified from a small contribution of surface water storage including wetlands in river basins with large inundation areas, such as the Amazon or the Mississippi. The results demonstrate the value of GRACE data and the multi-objective calibration approach for improvements of large-scale hydrological simulations, as they constitute a starting-point for improvements of model structure. The integration of complimentary observation data to further constrain the simulation of single storage compartments is encouraged.

1 Introduction

In the face of global climate change, forecasts about water shortage accumulate for many regions and water shortage becomes an increasing social-humanitarian prob-

lem. Global hydrological models are indispensable to track consequences of the alternating climate and to study the dynamics of water resources distribution. For a reliable monitoring of the stability and dynamical behaviour of the water cycle, changes in the water budget (change in total water storage $\Delta TWS=P-E-R$) of specific regions like large river basins play a key-role. To simulate the water cycle, hydrological models are forced by e.g., precipitation (P) and different climatic conditions, to estimate flow and storage of water on the continents and its charge to other Earth's subsystems like atmosphere and oceans by processes of evaporation (E) and runoff (R), respectively. A consistent representation of the continental water cycle and its components are a major issue for hydrological modelling. Only recently, however, variations of TWS have become a key variable in evaluating large-scale models (Güntner, 2009).

Several large-scale or global hydrological models exist (see Dirmeyer et al., 2006; Widen-Nilsson et al., 2007; Liu et al., 2007, 2009; Milly and Shmakin, 2002; Rodell et al., 2004), but estimates of variations in the total water storage (TWS) differ largely between them. Werth et al. (2009b) compared global TWS variations (TWSV) of the conceptual WaterGAP Global Hydrological Model (WGHM) with two physically based land surface models (the Global Land Data Assimilation System, GLDAS and the Land Dynamics model, LaD) and discovered differences in the magnitude of the signal itself between the three models, though temporal correlations are high. Reasons are different input data and modelling strategies for representing storage and flow processes at the coarse scale. Also, there is still a lack of knowledge about the regional importance and characteristics of individual storage processes. For example, surface water storage or deeper groundwater are absent or inattentively treated in many land surface models (Güntner, 2009; Niu et al., 2007).

Syed et al. (2008) assessed TWS variability of GLDAS on the global scale being too small and concluded that the absence of groundwater and surface water or uncertain snow parameterizations were possible reasons for model errors. For the land surface model ORCHIDEE, TWS amplitudes and phases could be improved by introducing a cumulative surface water and groundwater reservoir that allowed for a longer

residence time of water in the river basins (Ngo-Duc et al., 2007). Recent regional studies focus on modelling of groundwater storage with land surface models (e.g., Gulden et al., 2007; Lo et al., 2008; Kollet and Maxwell, 2008) but groundwater is still absent in several large-scale or global models. Although the global model WGHM simulates the most important storages compartments, including surface water and groundwater, simulation accuracy of the conceptual model was originally low for river discharge in snow dominated and semi-arid regions. Here, difficulties in the representation of evaporation or snow accumulation appeared (Döll et al., 2003). In response, Hunger and Döll (2008) and Schulze and Döll (2004) improved model equations for both processes. For TWS, however, WGHM still tended to underestimate seasonal TWS variations and phase shifts appeared (Schmidt et al., 2008b, 2006). Güntner et al. (2007) found a regional varying sensitivity of WGHM parameters. Since only one parameter of the original model has globally been calibrated so far, this calls for an extension towards a regional calibration with respect to dominant processes of a river basin.

Theoretical studies propagate an iterative working process of model prediction, model analysis and process understanding (e.g., Fenicia et al., 2008; Savenije, 2009). An evaluation of model predictions should be undertaken by comparisons of simulated states of the water cycle to real-world observations. Model behaviour during tuning processes like data assimilation (e.g., Houtekamer and Mitchell, 1998; Reichle et al., 2002) or model calibration (e.g., Duan et al., 2003; Gupta et al., 2005) provides information on process behaviour and structural model deficits. But, the learning process is especially difficult on the global scale and limited to iterative steps, primarily because of the lack of adequate model forcing and validation data with global coverage and acceptable resolution and accuracy.

In this respect, the Gravity Recovery And Climate Experiment (GRACE) is of extraordinary benefit for large-scale hydrological studies. With global coverage, monthly gravity observations from this twin-satellite-mission are transferable to the variability of water stored on and below the Earth's surface with a resolution of a few hundred kilometres (e.g., Tapley et al., 2004; Wahr et al., 2004). After removal of atmospheric

and oceanic gravity effects, GRACE observations enable temporarily reliable studies of different hydrological processes (like snow and ice, groundwater, soil, surface, as done by Wouters et al., 2008; Niu et al., 2007; Swenson et al., 2008; Papa et al., 2008, respectively) that include different climatic conditions and extreme events for many re-
5 gions (e.g., Zeng et al., 2008; Seitz et al., 2008) or the water balance itself (Sheffield et al., 2009). Since the first GRACE record became available, large progress has been made in order to improve GRACE data accuracy and, thus, the reliability of water mass variations from GRACE. These include studies on dealiasing (Han et al., 2004), error estimates (Horwath and Dietrich, 2006), development of filter (Swenson and Wahr,
10 2002) and decorrelation techniques (Kusche, 2007) as well as filter optimization (Werth et al., 2009b). Consequently, GRACE depicts a valuable tool for validation and calibration of large-scale hydrological models (Schmidt et al., 2008a; Güntner, 2009; Lettenmaier and Famiglietti, 2006). Application of GRACE data for large-scale hydrological modelling started out with validation of simulated water storage variations for large river
15 basins or with global coverage (e.g., Ngo-Duc et al., 2007; Syed et al., 2008; Güntner, 2009). More recently, promising further steps were made towards the integration of GRACE data into model development and model tuning for particular regions, e.g., the Amazon or Mississippi basin (e.g., Zaitchik et al., 2008; Werth et al., 2009a; Lo et al., 2009). As a subsequent step that makes full use of the global coverage of GRACE,
20 a world-wide integration of TWS variations towards an improved simulation of continental TWSV as a whole would be desirable. But many combinations of simulated single storage compartments may lead to a good fit for the integrative GRACE TWS variations with only coarse resolution. Hence, to obtain additional model constraints, higher parameter accuracy (Yapo et al., 1998; Vrugt et al., 2003; Gupta et al., 2005)
25 and to reduce parameter equifinality (Beven and Binley, 1992), the combination with other system states, like river discharge, in a multi-objective method is promising. In addition, using GRACE-based TWSV and river discharge is of particular interest for water balance analyses as both are integrated measures of the hydrological dynamics in a river basin.

In this context, this study makes a step forward in the iterative learning process of large-scale hydrological modelling towards improved global simulation of the continental water cycle and its storage compartments by a multi-objective calibration (Sect. 2.2) of the global model WGHM (Sect. 2.1) against river discharge and GRACE-based estimations (Sect. 2.3) for 28 of the largest and most important river basins world wide (Sect. 3.1).

2 Methods and data

2.1 Global hydrological model

The WaterGAP Global Hydrology Model (WGHM, Döll et al., 2003) simulates the continental water cycle by conceptual formulations of the most important hydrological processes. WGHM was originally developed by Döll et al. (2003) for water availability studies at the continental scale (Alcamo et al., 2003, e.g.,). But since the model provides estimates of water masses, it may serve for for hydrological analyses of water storage and its global dynamics (Güntner et al., 2007) as well as for individual storage compartments, such as groundwater recharge (Döll and Fiedler, 2008) or storage of surface water bodies (Papa et al., 2008). WGHM was numerously applied for comparison of continental water storage variability to GRACE-based water mass variations (Schmidt et al., 2006, 2008b).

The conceptual model equations of WGHM are described in detail by Döll et al. (2003), Kaspar (2004) and Hunger and Döll (2008). In general, if water precipitates as rain it is passed through the storages of interception, surface water (including rivers, reservoirs, lakes and wetlands), soil and groundwater, reduced for evapotranspiration losses. In case of precipitation falling as snow, it accumulates as snow storage and follows the above liquid water cycle after melting. Additionally, human water consumption is considered (Döll et al., 2003). Accumulation of ice or permafrost is not accounted for in WGHM (Hunger and Döll, 2008). The model is computed on a daily time step

and cell-wise with a 0.5° spatial resolution, excluding Antarctica and Greenland, hence, 66896 grid cells world wide. The water passes from cell to cell according to a global drainage direction map (Döll and Lehner, 2002) until it reaches a coastal cell, where it discharges to the oceans. The simulations of the hydrological cycle are supplied by
5 cell-based information on properties of soil, land cover, hydrogeology as well as on locations of reservoirs, lakes and wetlands (Döll et al., 2003).

A very recent version of WGHM as described by Hunger and Döll (2008) with updates for the input data for surface water bodies and human water consumption, an improved snow algorithm and a more realistic formulation of evaporation of lakes and wet-
10 lands was used in this study. To allow model runs for the GRACE period (2002–to date), the model was forced by climate data (temperature, cloudiness and number of rain days per month) from the operational forecasts of the European Centre for Medium-Range Weather Forecasts (ECMWF). Monthly precipitation input from the Global Precipitation Climatology Centre (GPCC) was used. Precipitation data were corrected for precipi-
15 tation measurement errors according to Legates and Willmott (1990) following Fiedler and Döll (2007). This model set up formed the reference of the present study and is hereafter called the *original model version*.

Döll et al. (2003) and Hunger and Döll (2008) tuned the original WGHM against long-term river discharge by a runoff coefficient parameter, which determines the frac-
20 tion of effective precipitation that translates into runoff, depending on the saturation of soil water (Eq. 3, Döll et al., 2003). Both studies noted that calibrating this parameter only was not sufficient for some areas to get acceptable simulation results for river discharge because, for instance, the water balance of lakes and wetlands is not influenced by this calibration approach, and because of other mis-modeled processes.
25 Therefore, this study intends to calibrate WGHM parameters of all important process formulations besides runoff within a river basin (see Sect. 2.2.1). We consider calibrated parameter values as effective values that account for non-resolvable features in a large-scale model such as sub-scale variability, input data errors, model structure errors or simplifications in model equations.

Printer-friendly Version

Interactive Discussion

WGHM consists of 36 model parameters. They are explained in detail in the publications of the original model versions while an overview of the 21 relevant WGHM parameters for this study is given below and in Table 1. The admitted parameter ranges for calibration were based on literature data and qualitative reasoning (Kaspar, 2004).

⁵ The soil storage capacity depends on the soil type and the land cover and is regulated by the *root depth* parameter. This parameter is calibrated as a multiplicative factor (SL-1), i.e., the particular value for soil storage capacity based on the soil and land cover data in each model cell is multiplied by the value of SL-1 (here in the range of 0.5 to 2, see Table 1). Groundwater storage and outflow is governed by the *ground-*
¹⁰ *water baseflow coefficient* (GW-1).

Surface water transport may on the one hand be calibrated by the *river velocity* (SW-2). On the other hand, the *surface water flow coefficient* (SW-5) as well as the maximum range of water levels in lakes (*lake depth*, SW-3) and wetlands (*wetlands depth*, SW-4) determine storage rates of surface water bodies and are possible calibration
¹⁵ parameter for surface water transport processes. Furthermore, the *runoff coefficient* parameter, which was tuned against river discharge for the original model versions, is calibrated as a multiplier (SW-1) in this study.

The potential evapotranspiration is computed in WGHM by the approach of Priestley and Taylor (1972) (PT). The equation is adjusted by the *PT-coefficient* that differenti-
²⁰ ates between humid (average relative humidity of 60% or more, ER-5) and arid regions (average relative humidity less than 60%, ER-6). The net radiation required as input for the PT-approach is computed according Shuttleworth (1993) (see Döll et al., 2003). Herein, the *radiation proportion* parameter (ER-1) is used to determine the radiation fraction of the extraterrestrial radiation that reaches the Earth's surface. The radiation
²⁵ fraction may be reduced by cloud cover following a *radiation correction* parameter (ER-2). The actual evaporation of open water can be calibrated by the *open water albedo* (ER-4) and sublimation of snow by the *snow albedo* (ER-3). Land surface evapotranspiration is limited by the *maximum potential evapotranspiration* (*MPET*, ER-7) parameter (see Döll et al., 2003).

Interception storage capacity depends on three parameters: The *maximum canopy water height* (*MCWH*, IN-1) as well as a *specific leaf area multiplier* (IN-2) and a *biomass multiplier* (IN-3).

The rates of snow melt and accumulation depend on land cover and elevation. Snow melt is computed in WGHM by a degree-day approach. The *degree-day factor* depends on the land cover type. It is calibrated in this study by a multiplicative factor (SN-3). Sub-grid variability of elevation within a 0.5 degree model cell is represented in WGHM (100 sub-units per 0.5°-cell) and elevation effects are accounted for by a *temperature gradient* (SN-4). Additional effects on snow storage processes can be adjusted by a cell-averaged *snow freeze temperature* (SN-1) and *snow melt temperature* (SN-2).

2.2 Calibration technique

2.2.1 Calibration regions and parameter sensitivity

Due to the limited resolution of GRACE data, the 28 largest and most important river basin worldwide were selected for this study (Fig. 1). Except for Volta in western Africa, all basins are larger than $600\,000$ km^2 in size (see Table 2). WGHM calibration is carried out separately for each basin.

Güntner et al. (2007) showed that WGHM parameter sensitivity for water storage variations varied between the river basins. This inter-basin variability is due to different climatic conditions as well as land surface properties and, thus, varying relevance of different storage processes. Consequently, for each region, only the sensitive parameters should be calibrated in order to reduce computational costs and to simplify the interpretation of the calibration results. A sensitivity analysis (SA) against TWSV and river discharge was undertaken (see also Werth et al., 2009a) following the SA approach of Hornberger and Spear (1981). The parameter sensitivity was analyzed by a Latin Hyper-cube sampling for 2000 parameter sets for all 28 river basins. Applied parameter ranges are given in Table 1. The resulting six to eight most sensitive parameters for TWSV and river discharge (Table 3) were used for the regional calibration of

each river basin and non-sensitive parameters were set to their original values (Table 1, col. 3).

The results of the SA confirmed that the subset of sensitive parameters varied considerably between the river basins. While snow parameters are not sensitive in tropical basins, parameters that control surface water transport appeared as particularly sensitive in basins with important flood plains, such as the Amazon. A broader range of sensitive parameters resulted, for instance, in the Indus river basin which is, on the one hand, dominated by snow storage in the northern mountain area and, on the other hand, high evaporation rates in desert region of the lower Indus. Hence, sensitive parameters belong to these two processes and, e.g., soil water parameters are comparatively less important in the Indus basin. As an example of a river basin that stretches among three different climate regions (cold in the north, subtropical in the southeast and dry in the southwest), important parameters for the Mississippi cover a variety of processes (soil, snow, evaporation, interception and surface water).

2.2.2 Multi-objective calibration approach

The multi-objective calibration approach of WGHM was explained in detail by Werth et al. (2009a). Figure 2 and the description below gives an overview. The calibration was done for all 28 river basins in an automated framework for the period 01/2003–12/2007.

Calibration is a widely used optimization technique in hydrological modelling. In an iterative process, different parameter values are tested for their ability to generate model system states that fit well to observations. The best parameter set provides the lowest simulation error or the highest simulation performance expressed by an objective value. Several functions to measure the objective value are possible, like the normalized root mean square error or the correlation coefficient. Within this study, the Nash-Sutcliffe-efficiency coefficient (NSC, Nash and Sutcliffe, 1970) is applied. NSC is a simulation performance measure that normalizes the squared difference of a predicted to an observed time series by the sum of squared deviations of the observations to their mean

during the period of interest. It ranges from $-\infty$ to 1 (optimal fit), with a value of 0 indicating a simulated time series that performs as well as a model being equal to the mean of the observable. NSC is applied here because it measures errors in phase, amplitude and mean of a simulated time series at the same time.

5 Within a multi-objective calibration, more than one observation is applied to evaluate the model simulations, which makes the selection of the best parameter set less trivial. Due to errors in the model structure and the input data (Vrugt et al., 2003), the approach will no longer provide one single optimal parameter set, but lead to a Pareto set of optimal solutions (Gupta et al., 1998). Each Pareto solution provides a better
10 simulation performance than any other Pareto solutions for at least one of the objectives (but not all objectives). Without additional information on the observations or a defined priority of simulation accuracy, the Pareto solutions are equal. In this study, river discharge and TWSV were applied for the calibration of WGHM and a balanced improvement of simulation performance for both objectives was intended. Therefore,
15 the solution closest to the optimum of the objective values (here a value of NSC=1 for both objectives) was selected as the best parameter set and used for further analyzes.

For parameter variation, ranking and archiving the calibration algorithm ϵ-Non-dominated Sorting Genetic Algorithm-II (ϵ-NSGAII, Kollat and Reed, 2006) was used. The multi-start scheme and the evolutionary strategy of the algorithm (mutation,
20 crossover and selection) enable a global optimization of the parameter values and are able to solve highly non-linear optimization problems. The algorithm is one of the most efficient and effective multi-objective optimization methods used in hydrological modelling (Tang et al., 2006). These features enable a multi-objective calibration for more than one parameter of the non-linear and computational expensive WGHM model sys-
25 tem. ϵ-NSGAII operators were set to values proposed by Kollat and Reed (2006) and a population size of N=12, an ϵ-resolution of 0.05 for both objectives and a generation size of 100 (hence, a maximum of 1200 model evaluations) were used.

In contrast to Werth et al. (2009a) who applied significant signal periods within the GRACE data for their calibration, a calibration against full time series of GRACE TWSV

was undertaken in the present study (see data Sect. 2.3). During the calibration of WGHM, TWSV simulations were filtered in the same way as GRACE data (see Sect. 2.3.2 and Table 2) to ensure equal resolution and a consistent comparison of both data sets.

2.3 Calibration data

2.3.1 Discharge data

River discharge data of the most downstream gauging station of each river basin were used (Table 2, col. 4 and Fig. 1). Data were obtained from the Arctic Regional Integrated Hydrological Monitoring System for the Pan-Arctic Land Mass (ArcticRIMS, http://rims.unh.edu), the Environmental Research Observatory for geodynamical, hydrological and biogeochemical control of erosion/alteration and material transport in the Amazon (ORE HYBAM, http://www.ore-hybam.org) and the Global Runoff Data Center (GRDC, grdc.bafg.de).

For the Amazon, Mississippi, Mackenzie, Ob and Yenisei monthly discharge data were available for the GRACE operation period. For all other basins, up-to-date measurements were not available and mean monthly river discharge (for Jan-Dec) was computed from the most recent period of available data (maximum period of 30 years, see Table 2).

Errors of discharge measurements depend on the individual measurement methods and channel cross sections are likely to vary for the individual stations and time periods. Unfortunately, no details are provided from the data centres on the accuracy of discharge measurements. Therefore, the error of discharge measurements was set to a conservative value of 20% for the uncertainty analysis of the calibration results.

2.3.2 GRACE data

The greatest challenge in the application of GRACE-based TWSV is marked by the difficulty of separating error from signal as well as separating signal from the region of interest and its neighbouring regions. The spatial resolution of the GRACE data is limited due to the decreasing sensitivity of the satellites to mass variations with smaller geographical extent. Simulation data of atmospheric and oceanic circulation models are applied to de-alias the gravity fields from sub-monthly circulation effects in both systems. Errors in these de-aliasing data and satellite measurement errors increase the noise in spherical harmonic coefficients particularly for higher degrees of the expansion terms, i.e., higher spatial resolution (e.g., Schmidt et al., 2008a). The error budget is also influenced by signal leakage errors from surrounding areas. As a consequence, the application of filter methods is indispensable to reduce noise in the GRACE data. Nevertheless, the magnitude of errors varies between particular regions and months. Therefore, the user has to decide on an adequate filter method as well as for filter parameter settings to balance and minimize GRACE measurement errors and leakage errors. Filtering in turn may change the final signal properties. Werth et al. (2009b) showed that filter induced amplitude damping and phase shifts in time series of basin-averaged TWSV differs between regions because of varying signal characteristics inside and outside of the river basin and basin shape. Hence, the selection of an optimum filter method is a function of the river basins. For the present study, the optimal filter methods (and parameter values) of Werth et al. (2009b) were applied for smoothing of GRACE and hydrological data in 22 river basins. For the remaining six basins (Columbia, Huang He, Mekong, Murray, Orinoco and Volta) optimum filter settings were derived by repeating the method of Werth et al. (2009b) (see Table 2 for a summary of applied filter methods).

The method to transform the spherical harmonic representation of GRACE gravity data to regional averaged water mass variations by Swenson and Wahr (2002) was applied using river basin boundaries as displayed in Fig. 1. Long-term trends deter-

Title Page

Abstract | Introduction

Conclusions | References

Tables | Figures

◄ | ►

◄ | ►

Back | Close

Full Screen / Esc

Printer-friendly Version

Interactive Discussion

mined both from the hydrology model WGHM and from the GRACE gravity fields were removed from time series of TWSV in this study.

GRACE derived time series of TWSV from different processing centres show significant differences (as for the Lena basin in Fig. 3). These differences are due to different processing strategies, background models or processing software (Schmidt et al., 2008a) and reflect uncertainties in the GRACE data. Consequently, an average of GRACE gravity fields (Level-2 products, most recent version RL04) from three processing centres was used (Flechtner, 2009): the German Research Center for Geosciences (GFZ, until degree 120), the Center for Space Research (CSR, until degree 60) and the Jet Propulsion Laboratory (JPL until degree 120). The three sets of coefficients were averaged from degree 2 to 60 for each month in the period from 02/2003 until 12/2008, excluding 06/2003 and 01/2004 due to missing data from GFZ. For GFZ, regularized solutions for 07–10/2004 and 12/2006 were applied.

GRACE errors were estimated from the error coefficients of the individual data sets published by the processing centres, i.e., correlated errors as provided by GFZ and CSR (Schmidt et al., 2008a; Wahr et al., 2006). As correlated errors were not available for JPL gravity fields, the confidence interval of JPL coefficient errors is increased to 99% by assuming a normal distribution. This results in a multiplication by ≈ 2.6 of the formal coefficient errors. The final error estimates for the averaged coefficients from the three processing centres amounts to:

$$e_{knm}^{\text{avefield}} = \sqrt{e_{knm}^{\text{GFZ}2} + e_{knm}^{\text{CSR}2} + e_{knm}^{\text{JPL}\,2}}, \, k = [0, 1], \, n = [2, 60], \, m = [0, 60]. \tag{1}$$

Errors in the coefficients are propagated to the basin averages of water storage for each river basin. See Fig. 3 for an example of basin-averaged TWSV derived from the three gravity solutions, the average solution and associated errors.

2.4 Uncertainty estimation due to observational errors

The uncertainty of the calibration results due to errors in the calibration data is estimated for each river basin by the following procedure: 1) Selection of the calibration run with the Pareto solution closest to the optimum (see an example for the Lena river basin in Fig. 4). 2) Propagation of GRACE coefficient errors to basin-averaged estimates of TWSV as well as determination of the 20% discharge error. 3) Generation of 5000 normally distributed samples within the estimated error ranges for the monthly data points of GRACE-based TWSV and monthly river discharge, respectively. The sample size was tested ahead and selected to provide stable statistical results. 4) Estimation of both objective functions (NSC) for each sample against simulated time series of the selected optimal solution, respectively for TWSV and discharge. 5) Determination of the NSC standard deviations for both objectives as the semiaxis for an error ellipse around the selected optimal solution. And 6) Selection of all calibration runs within the error ellipse (see Fig. 4 for the Lena basin).

The described approach determines all Pareto solutions around the selected optimum and non-Pareto solutions close to the Pareto frontier, which cannot be evaluated to provide a better fit to the observations than the selected Pareto solution if the error range of the observations is considered. The selected cluster of calibration solutions represents the total uncertainty of the calibration results in view of the observation errors.

3 Results and discussion

3.1 Calibration results

Detailed results for Lena basin (Fig. 4) show a typical objective function response that was found after calibration of most river basins. A clear trade-off exists between both objective functions for TWSV and mean monthly discharge. The best solutions for the

single objectives are located at the end of the Pareto frontier (crossed dots). Best results for a single objective, however, give an undesirable decrease in the accuracy for the other objective. The selected Pareto optimum (large gray dot) provides a balanced improvement between both objectives. The multi-objective calibration approach also decreases equifinality of the parameter sets, since unacceptable parameter sets for any of the objectives are excluded by the multi-objective evaluation scheme. A more pronounced equifinality for simulating total water storage variations originates from the character of total water storage data. Since GRACE provides no absolute values but only variations of water masses, the same storage variations may be simulated by different model representations with different absolute amounts of water stored in the river basin. This is not the case for river discharge where both absolute values and variations are given by the observation data. Hence, a smaller number of model realizations provides good objective values for evaluation by discharge than by TWSV. The large ellipse around the selected Pareto optimum represents its uncertainty caused by measurement errors in the calibration data. Variations of parameter values or model output for model realizations within this range are not significant for the assumed observation data errors. Nevertheless, a significant improvement was achieved for both objective values relative to the original model for the example of the Lena basin.

An overview of the calibration results for all river basins is given in terms of relative root mean squared error (RMSE, Fig. 5). The relative RMSE was computed from the RMSE of time series of mean monthly discharge (circles) and TWSV (squares) against root mean squared (RMS) values of the respective measurements. Absolute values of signal RMS and model RMSE are presented in Table 4. Uncertainty ranges due to observational errors were transferred to RMSE and relative RMSE values and they are indicated by error bars in (Fig. 5). A comparison of the results for the calibrated model (black symbols) and the original model (gray symbols) indicate a successful calibration with significant improvements for both objectives for most of the basins. The highest relative improvement of TWSV simulations are provided (and respective RMSE improvements as height of a water column) for the Amazon (ca. 24 mm), Danube

(7 mm), Lena (4 mm), Mekong (13 mm), Mississippi (8 mm), Volga (13 mm) and Zambezi (15 mm). Mean monthly discharge simulations improved in particular for the Amazon (with 10 km^3/month decrease in RMSE), Danube (3 km^3/month), Niger (14 km^3/month), Tocantins (10 km^3/month) and Volga (18 km^3/month). For Huang He, Indus and Mekong, improvements were achieved for TWSV simulations only. For the first two of these basins, discharge accuracy is of the same level for the calibrated compared to the original model and the accuracy decreased slightly for Mekong. But the discharge simulations of all three basins are within the measurement error bands. Nelson, Orange, Yukon and Congo (Zaire) exhibit an improvement of discharge simulations while TWSV simulations are of the same performance as for the original model.

With the selected optimum parameter sets, WGHM simulations were repeated between 01/2008–12/2008 beyond the calibration period for validation against GRACE-based TWSV. Table 4 shows that the improvement relative to the original model is similar to the calibration period for most of the river basins. For example, RMSE differences to the original model are promising for the Amazon (31 mm), the Lena (10 mm), Mackenzie (10 mm), Mekong (14 mm), St. Lawrence (19 mm) or Zambezi (25 mm). For Murray, Nelson, Orange and Yenisei only a slight improvement for TWSV simulation is achieved in the validation period. A larger RMSE than for the original model was found for Ganges, Huang He, Indus, Orinoco, Nelson, Orange and Congo. This corresponds to the calibration failure of the latter three basins mentioned above.

3.2 Simulation of seasonal TWSV

The effects of model calibration on seasonal amplitudes and phases of TWSV are given in Fig. 6. For the most basins, the amplitude was shifted towards the GRACE observations. The strongest improvements for the seasonal amplitude are achieved, e.g., for Amazon, Mackenzie, Niger, Orinoco and Zambezi. For some basins, reduced seasonal phase differences between GRACE and WGHM could be achieved by calibration (e.g., Amazon, Mississippi, Ob and Congo). Only phases could be corrected for Columbia, Danube, Lena, Nelson, Parana and Yenisei. No success for the calibration results

again for Huang He in case of the seasonal signal. For Amur and Orange phases differ strongly between GRACE and WGHM, but TWS does not exhibit a distinct seasonal signal in both basins (not shown).

3.3 Parameter values and single storage compartments

A detailed analysis of parameter changes (Fig. 7) and their effects on single storage compartments (Figs. 8–9) is provided below for the example of seven river basins of different continents, climatic conditions and calibration success. Storage in lakes, floodplains and wetlands (denoted surface water) is analyzed separately from water in the river channel (denoted river storage) in the following sections.

Amazon

The better representation of TWSV simulations for the tropical Amazon after multi-criterial calibration is mainly due to a lower river flow velocity (SW-2) in the calibrated model version as well as a larger runoff coefficient (SW-1). The adjustment of both parameters is stable against calibration uncertainty from observation errors (Fig. 7a). The parameter changes cause a longer-lasting storage of more water in the river network which leads to larger and delayed seasonal amplitudes of TWS in line with GRACE observations (Fig. 8a). Also, inter-annual variations of TWS such as a heavy drought experienced in the Amazon in 2005 (Zeng et al., 2008) are better represented with the calibrated model (Fig. 8a). A slightly increased soil water storage is due to the larger rooting depth (SL-1) in the re-calibrated model. But the rooting depth parameter is highly uncertain and it is not significant relative to the original model as can be seen from the wide spread of parameter values for the Pareto solutions in Fig. 7a. The larger value of the parameter wetland depth (SW-4) has nearly no effect on the storage variability in lakes and wetlands in spite of the large importance of wetlands and floodplains for water storage in the Amazon (e.g., Papa et al., 2008). Surface water storage is mainly attributed to river channel storage in WGHM (Fig. 8a)

although the large inundation areas are taken into account as model input. This may indicate structural model errors in representing surface water exchange processes between floodplains and the channel due to the conceptual model formulations and the cell-based simulation of surface water bodies in WGHM.

Mississippi

The Mississippi basin is located in different climate zones ranging from cold to temperate (Fig. 1) and therefore it shows a more complex contribution of the individual storage compartments (see Fig. 8b) than the Amazon. The most important change in TWSV after model calibration is due to a larger soil storage variability and a longer storage persistence in the early summer, caused by a deeper rooting depth (SL-1). Secondly, a higher snow melt temperature (SN-2) causes an increased snow peak and later melting by one month. The changes for snow and soil storage are supported by a lower radiation proportion absorbed by the surface, which leads to higher snow accumulation as well as a delayed snow melt. These parameter changes for the Mississippi compared to the original model are reliable considering calibration uncertainty (Fig. 7d). An earlier seasonal peak of simulated TWS compared to GRACE data (see Fig. 8b) can possibly be attributed to underestimated groundwater storage that are typically characterized by a later seasonal phase compared to near-surface storage. In fact, studies of (Rodell et al., 2007) and Zaitchik et al. (2008) indicate a higher groundwater volume than represented by WGHM. A change for groundwater was prevented by the missing sensitivity of groundwater parameter for WGHM (B11 in Table 3), which may be due to the overlap with soil storage variations. The groundwater parameters should therefore be included in further calibration studies.

Lena

For the Lena basin, the seasonality of river water storage exhibits an opposite

HESSD

6, 4813–4861, 2009

WGHM calibration analysis with GRACE

S. Werth and A. Güntner

Title Page

Abstract | Introduction

Conclusions | References

Tables | Figures

◄ | ►►

◄ | ►

Back | Close

Full Screen / Esc

Printer-friendly Version

Interactive Discussion

phase to total storage which is dominated by snow storage variations. This makes a fit of the overall small TWSV amplitude (below 50 mm w.eq. in average) more difficult than for the two previous basins. Model improvements by calibration for this cold, high-latitude basin (Fig. 1) mainly are of temporal nature. The phase of TWSV could be corrected (see also Fig. 6) based on changes of water accumulation in snow, river and soil (Fig. 8c). Due to a larger snow melt temperature (SN-2), snow accumulation lasts nearly one month longer while snow melt finally occurs later but more rapidly in April and May. The larger snow albedo (ER-3) decreases snow sublimation and supports the slightly larger variability of snow storage. In line with the later and faster snow melt in spring, water storage dynamics in river network change accordingly. A larger and later monthly runoff peak also corresponds to the river discharge measurements and is better represented by the calibrated model (see embedded graph in Fig. 8c). Changes in soil storage dynamics due to calibration are of minor importance in the Lena basin but, in general, are characterized by slightly larger seasonal variations with a later phase commensurate to the snow dynamics but also to overall lower evapotranspiration rates caused by smaller radiation proportion (ER-1) and PT-coefficient (ER-5) parameters.

Danube

As for Lena, mainly a phase correction of TWSV was achieved by calibration (Fig. 6) for the cold and partly temperate (Fig. 1) Danube basin. This resulted in a smaller RMSE of TWSV time series (Fig. 5). While the seasonal amplitude was not changed, a better fit of extreme events like heat waves or floods as observed by Andersen et al. (2005); Seitz et al. (2008) are visible in the time series for autumn of 2003, 2005 and 2006, as well as for the water mass maxima in 2004 and 2006 (see Fig. 8). In the calibrated model, snow is melting faster due to a higher snow melt temperature, hence reducing the snow storage volume. The released water is mainly stored in the soil of which the storage capacity was increased by a larger root

depth parameter after calibration. Also river water is reallocated to the soil where it can remain for longer periods during the spring season than in the quickly draining river network. The smaller river discharge in spring is confirmed by observations (not shown here, due to limited space), hence, a smaller RMSE for mean monthly discharge (Fig. 5). Groundwater storage variations slightly decreased and delayed in the Danube basin.

Zambezi

Increased storage variations in the hot-temperate and partly dry Zambezi basin (Fig. 1) are due to larger soil, groundwater and surface water storage amplitudes (Fig. 9a). The largely corrected seasonal variability of TWSV (Fig. 6) in the calibrated model originates mainly from less evapotranspiration of surface and soil water as controlled by a smaller PT-coefficient (ER-6) and a smaller maximum potential evap-otranspiration (ER-7). As WGHM contains only one soil layer, it may be exhausted too quickly by evapotranspiration in the dry Zambezi region instead of being stored in deeper soil layers. This is supported by the increased groundwater volume, that confirms the high relevance of water exchange with deeper soil zones for Zambezi basin (see also Winsemius et al., 2006a). Surface water volume changes in wetlands increase after calibration and cause longer residence times of water in the Zambezi basin. The importance of this storage mechanism in the Zambezi basin was also found by Winsemius et al. (2006a).

Nelson

The seasonality of snow and groundwater storage exhibits a marked anti-phase in the Nelson basin according to the WGHM simulation results (Fig. 9b). This decreases model sensitivity for TWS variations and makes an effective calibration of the individual storage components difficult, since many combinations of different snow

and groundwater states can lead to an equally good fit of simulated to GRACE-based TWSV. In addition, the required smoothing of GRACE data has a huge effect on overall water storage dynamics for this basin (Fig. 9). Major seasonal signals are smoothed out, but remaining TWSV time series correspond reasonably well between GRACE and WGHM. Comparatively small changes occur by model re-calibration relative to the original model.

Congo

TWSV in the Congo (Zaire) basin is dominated by inter-annual patterns such as a water loss between 2003 and 2005 as described before by Crowley et al. (2006). But as assumed by these authors, the loss is not of secular nature and the storage is filled up again during 2006 and 2007 (Fig. 9c). Though the calibrated WGHM exhibits an improved simulation for seasonal amplitude and phase of the Congo basin (Fig. 6), the simulated inter-annual variability of basin-average TWS is still different from GRACE, e.g. a too large negative anomaly in 2005. Also, RMSE values did not improved after calibration (Table 4). The inter-annual variations in TWS mainly derive from soil and groundwater storage (Fig. 9c). For the calibrated model, a larger seasonal variability in soil storage causes a slightly delayed phase of storage variability. This delay appears to be compensated by a negative phase shift in groundwater. As a result, the faster outflow of the groundwater (due to a larger outflow coefficient GW-1) causes a smaller groundwater volume and decreases the inter-annual variation of groundwater storage in the calibrated model.

Three of the four basins (Nelson, Orange, Congo) with an unsuccessful calibration for TWS exhibit strong inter-annual variations (see Fig. 9b, c for Nelson and Congo). The inter-annual variations are visible in GRACE as well, but the short period of five years used here may impede the effective calibration of inter-annual changes in total storage variability and its components. Furthermore, for Congo, Nelson and Orange a large trade-off occurs for the Pareto solutions between simulation performance of river

Back | Close

Full Screen / Esc

Printer-friendly Version

Interactive Discussion

discharge simulation and TWS (not shown). Therefore, calibration difficulties within these basins may also be due to the use of mean monthly discharge values, which neglect inter-annual variations during the calibration period. As a further drawback for Congo, available discharge data are from the period 1954–1983 for this basin.

The water mass variation of the Orange basin, which also exhibit inter-annual variations (not shown), are smaller than 12 mm of a water column (see Table 4 and Fig. 6) and for some months below GRACE data accuracy. While inter-annual variations are not relevant for the Yukon basin, similar to Nelson, a clear anti-phase between snow and groundwater storage as well as soil storage causes a small model sensitivity for TWS variations.

3.4 Global analysis

A global analysis of simulated TWSV for the calibrated model (see spatial distribution in Fig. 10 and variability of basin averages in Table 5) shows that its variability increased for the most river basins compared to the original model. On the global average (last row of Table 5), TWS variability increased by 7 mm w.eq., which is mainly due to a larger variations of soil, river and surface water storage. Most variability is gained within the tropical and temperate regions, like the Amazon (total 60 mm for the basin average), Congo (9 mm), Niger (14 mm), Mekong (35 mm) as well as for the Mississippi (14 mm). A spatial redistribution between sub-regions for some of these basins is visible in Fig. 10, e.g., Ganges and Parana. A smaller total water budget appears only for basins in cold regions like Mackenzie, St. Lawrence, Volga or Yangtze (Table 5). Some further cold regions like Lena or Ob exhibit an unchanged water budget. This comparison shows that TWS variability in the original WGHM was mainly underestimated in tropical and temperate regions but overestimated in cold regions, similar to the seasonal components (Fig. 6).

For the individual basins and storages, largest differences to the original model occur within soil storage, mainly for tropical and temperate regions like Mekong, Mississippi, Orinoco, Volta or Zambezi, which is visible by area distributed TWSV differences to the

original model in the lower Fig. 10 and reflected in the basin-averages (Table 5). Soil has the highest seasonal capacity to store water and contributes most to the gravity signal discovered by GRACE that is usually dominated by seasonal features. Linear structures in the spatial distribution TWSV differences to the original model are mainly due to changes in river storage, being the second most contributor to changes for the basin-averages (Table 5). Very large increase of river water volumes occur in rainy tropical regions of Amazon, Mekong and Orinoco, where a slow discharge in the river network causes a longer maintenance of river water in the basin (see analysis for Amazon in Sect. 3.3 above). In contrast, a decrease of river water volume is visible for temperate and dry regions. Snow storage increases for regions in cold climate zones e.g., Columbia, Ob, Yenisei). But it decreases for cold climates with a warm summer (St. Lawrence, Volga, Danube). In these transition zones, less snow precipitation may be due to global climate warming, that is relevant for the calibration period but not incorporated in the calibration of the original model.

Simulated groundwater storage changes decreased on the global scale. A large decrease of groundwater variations occurred for regions with a distinct dry season (Ganges, Niger, Nile) and for some cold regions (St. Lawrence, Volga). Groundwater seasonality is usually delayed compared to soil and surface storage, because groundwater recharge and runoff are temporarily filtered by soil transfer processes. As seen from seasonal phase shift between GRACE and WGHM, water often drains too quickly from river basins compared to GRACE even for the calibrated model version. This may be explained by a too small groundwater recharge and volume in WGHM (e.g. Zambezi or Mississippi). Also the sensitivity of the model to changes in groundwater storage may be superimposed by the soil storage with a different seasonal phase. Therefore, future calibrations against GRACE data should include groundwater timing and volume parameters for each river basin.

4 Conclusions

This study demonstrates that a multi-objective calibration with TWS variations from the GRACE satellite mission and river discharge enables a world-wide improved simulation of changes in the continental water cycle and its compartments. The presented strategy for improving simulations of continental water storage includes the following key points: 1) Inclusion of the most important storage compartments (soil, snow, canopy, rivers, surface water and groundwater) in the simulation of continental water storage for a comparison with satellite observations. 2) Multi-objective calibration by absolute values of river discharge and relative values of TWS variations. 3) Basin-specific calibration of dominant processes, hence of the most sensitive model parameters. 4) Assuring consistency of observables and model state variables (equal spatial scale) by identical smoothing of GRACE and model data, as well as the application of most optimal filter method for each river basin. 5) Consideration of measurements errors in an uncertainty analysis of the calibration results. 6) Analysis of calibration results to reveal model structural errors and to broaden the knowledge about hydrological processes on large-scales.

The multi-objective calibration of WGHM led to higher simulation accuracy for TWS variations and river discharge for most of the 28 calibrated river basins. Seasonal amplitudes and phases of the water budget for most river basins were improved. A global comparison showed that TWS variability was mostly increased for tropical regions. The highest proportion of the increase occurred for soil storage. An analysis of single storage compartments for seven river basins from different continents and diverse climatic regions revealed reasonable changes within single storage compartments of the calibrated model that contributed to a better representation of TWS variability. Herein, the deviation of the calibrated parameter sets to the original model version and their uncertainty due to measurement errors provide an insight into the control and reliability of the individual process simulations.

For some basins, possible model structural errors are uncovered by the calibration,

e.g., too small wetland volumes in the Amazon and the Mississippi basin. For some basins, errors or limits of the calibration data restrict the calibration success. An update of global river discharge data sets to the GRACE mission period is an urgent need for further progress. As another strategy for the calibration of basins with strong inter-annual variations and scarce discharge data availability, smaller weights could be given to mean monthly discharge data in the calibration process. However, the model representation of TWS variations inheres more parameter equifinality than river discharge due to the lack of absolute values and the integrative nature and limited spatial resolution of GRACE TWS variations. Consequently, GRACE data alone are not adequate for calibrating water storage state variables in large-scale hydrological models.

Calibration difficulties are also due to the complexity of interaction between single storage components and to the inability to separate these storages with the integrative TWSV data. Many different single storage combinations can lead to similar variations in the total water budget of a river basin. The decrease of model sensitivity for TWS or its components is catalyzed if clear anti-phases occur between storage variations in individual compartments. Since groundwater seasonality deviates mostly from the other storages, it plays an important role in the timing of TWSV in a river basin. A parameter sensitivity analysis for such basins should be undertaken carefully and for future studies, an increased attention should be given to groundwater storage in the calibration process.

The improvement of large-scale hydrological models and the validation of GRACE water mass estimates is an iterative process. Model structure errors may complicate the calibration of WGHM with GRACE TWSV. But also limited spatial resolution or regional varying accuracy (e.g., Winsemius et al., 2006b) as well as different smoothing effects between GRACE and modelled data may affect the calibration performance. Therefore, GRACE uncertainties are still an important object of research. Furthermore, due to the general data scarcity of hydrological observations at the global scale, newly developed observation systems like GRACE in turn depend on global model estimations for validation and error reduction. This will complicate the independence of

model re-calibrations and again it limits the application of GRACE for hydrology (and vice versa) in the sense of an iterative learning process.

As consequence to the named difficulties, it is desirable to include further hydrological observations into the calibration and validation process. Only satellite data are in the run for large-scale hydrological modelling and the rise of satellite observation systems with global coverage are promising. Groundwater observations are not available with global coverage and this storage is not directly accessible by space techniques. But satellite observations of snow storage (e.g., by MODIS, Parajka and Blöschl, 2008), surface water (Papa et al., 2008) or soil moisture from the future satellite missions such as SMOS and SMAP are applicable for tuning or validation of large scale-hydrological models with more than two objectives.

Due to the large diversity of processes in different regions of manifold climatic conditions, global hydrological modelling is a challenging ambition. The present study expands experiences on representing hydrological processes on the global scale with a particular emphasis on water storage dynamics. The continuation of similar studies is motivated by the steadily improved accuracy of GRACE solutions and the future prospect of a GRACE-follow on mission. Longer time series of gravity data will in particular allow focusing on hydrological extremes, inter-annual variations and secular trends in both observations and modelling capabilities.

References

Alcamo, J., Döll, P., Henrichs, T., Kaspar, F., Lehner, B., Rösch, T., and Siebert, S.: Development and testing of the WaterGAP 2 global model of water use and availability, Hydrolog.

Sci. J., 48, 317–338, 2003. 4818

Andersen, O. B., Seneviratne, S. I., Hinderer, J., and Viterbo, P.: GRACE-derived terrestrial water storage depletion associated with the 2003 European heat wave, Geophys. Res. Lett., 32, L18405, doi:10.1029/2005GL023574, 2005. 4832

5 Beven, K. and Binley, A.: The future of distributed models: Model calibration and uncertainty prediction, Hydrol. Process., 6, 279–298, 1992. 4817

Crowley, J. W., Mitrovica, J. X., Richard, C. B., Tamisiea, M. E., and Davis, J. L.: Land water storage within the Congo Basin inferred from GRACE satellite gravity data, Geophys. Res. Lett., 33, L19402, doi:10.1029/2006GL027070, 2006. 4834

10 Dirmeyer, P. A., Gao, X., Zhao, M., Guo, Z., Oki, T., and Hanasaki, N.: GSWP-2: Multimodel Analysis and Implications for Our Perception of the Land Surface, B. Am. Meteorol. Soc., 87, 1381–1397, 2006. 4815

Döll, P. and Fiedler, K.: Global-scale modeling of groundwater recharge, Hydrol. Earth Syst. Sc., 12, 863–885, 2008. 4818

15 Döll, P. and Lehner, B.: Validation of a new global 30-min drainage direction map, J. Hydrol., 258, 214–231, 2002. 4819

Döll, P., Kaspar, F., and Lehner, B.: A global hydrological model for deriving water availability indicators: model tuning and validation, J. Hydrol., 270, 105–134, 2003. 4816, 4818, 4819, 4820, 4846

20 Duan, Q., Gupta, H. V., Sorooshian, S., Rousseau, A. N., and Turcotte, R.: Calibration of watershed models, American Geophysical Union, Washington, D.C, 2003. 4816

Fenicia, F., Savenije, H. H. G., Matgen, P., and Pfister, L.: Understanding catchment behavior through stepwise model concept improvement, Water Resour. Res., 44, W01402, doi:10.1029/2006WR005563, 2008. 4816

25 Fiedler, K. and Döll, P.: Global modelling of continental water storage changes - sensitivity to different climate data sets, Adv. Goesci., 11, 63–68, 2007. 4819

Flechtner, F.: GRACE Science Data System Monthly Report, February 2009, Tech. rep., isdc. gfz-potsdam.de, 2009. 4826

Gulden, L. E., Rosero, E., Yang, Z.-L., Rodell, M., Jackson, C. S., Niu, G.-Y., Yeh, P. J. F., and
30 Famiglietti, J.: Improving land-surface model hydrology: Is an explicit aquifer model better than a deeper soil profile?, Geophys. Res. Lett., 34, L09402, doi:10.1029/2007GL029804, 2007. 4816

Güntner, A.: Improvement of global hydrological models using GRACE data, Surv. Geophys.,

29, 375–397, 2009. 4815, 4817

Güntner, A., Stuck, J., Werth, S., Döll, P., Verzano, K., and Merz, B.: A global analysis of temporal and spatial variations in continental water storage, Water Resour. Res., 43, W05416, doi:10.1029/2006WR005247, 2007. 4816, 4818, 4821, 4846

5 Gupta, H. V., Sorooshian, S., and Yapo, P. O.: Toward improved calibration of hydrologic models: Multiple and noncommensurable measures of information, Water Resour. Res., 34, 751–763, 1998. 4823

Gupta, H. V., Beven, K. J., and Wagener, T.: Model Calibration and Uncertainty Estimation, in: Encyclopedia of Hydrological Sciences, Part 11. Rainfall-Runoff Modeling, John Wiley &
10 Sons Ltd, 2005. 4816, 4817

Han, S. C., Jekeli, C., and Shum, C. K.: Time-variable aliasing effects of ocean tides, atmosphere, and continental water mass on monthly mean GRACE gravity field, J. Geophys. Res., 109, B04403, doi:10.1029/2003JB002501, 2004. 4817

Hornberger, G. M. and Spear, R. C.: An Approach to the Preliminary Analysis of Environmental
15 Systems, J. Environ. Manage., 12, 7–18, 1981. 4821

Horwath, M. and Dietrich, R.: Errors of regional mass variations inferred from GRACE monthly solutions, Geophys. Res. Lett., 33, L07502, doi:10.1029/2005GL025550, 2006. 4817

Houtekamer, P. L. and Mitchell, H. L.: Data Assimilation Using an Ensemble Kalman Filter Technique, Mon. Weather Rev., 126, 796–811, 1998. 4816

20 Hunger, M. and Döll, P.: Value of river discharge data for global-scale hydrological modeling, Hydrol. Earth Syst. Sc., 12, 841–861, 2008. 4816, 4818, 4819, 4846

Kaspar, F.: Entwicklung und Unsicherheitsanalyse eines globalen hydrologischen Modells., Ph.D. thesis, Universität Kassel, 2004. 4818, 4820, 4846

Kollat, J. B. and Reed, P. M.: Comparing state-of-the-art evolutionary multi-objective algorithms
25 for long-term groundwater monitoring design, Adv. Water Resour., 29, 792–807, 2006. 4823

Kollet, S. J. and Maxwell, R. M.: Capturing the influence of groundwater dynamics on land surface processes using an integrated, distributed watershed model, Water Resourses Research, 44, W02402, doi:10.1029/2007WR006004, 2008. 4816

Kusche, J.: Approximate decorrelation and non-isotropic smoothing of time-variable GRACE-
30 type gravity field models, J. Geodesy, 81, 733–749, 2007. 4817, 4847

Legates, D. R. and Willmott, C. J.: Mean Seasonal and spatial variability in gauge-corrected global precipitation, Int. J. Climatol., 10, 111–127, 1990. 4819

Lettenmaier, D. P. and Famiglietti, J. S.: Hydrology: Water from on high, Nature, 444, 562–563,

2006. 4817

Liu, J., Williams, J. R., Zehnder, A. J., and Yang, H.: GEPIC - modelling wheat yield and crop water productivity with high resolution on a global scale, Agricultural Systems, 94, 478–493, 2007. 4815

Liu, J., Zehnder, A. J. B., and Yang, H.: Global consumptive water use for crop production: The importance of green water and virtual water, Water Resour. Res., 45, W05428, doi:10.1029/2007WR006051, 2009. 4815

Lo, M.-H., Yeh, P. J.-F., and Famiglietti, J.: Constraining water table depth simulations in a land surface model using estimated baseflow, Adv. Water Resour., 31, 1552–1564, 2008. 4816

Lo, M.-H., Famiglietti, J. S., Yeh, P. J.-F., and Syed, T. H.: Improve parameter estimation and water table depth simulation in a land surface model using GRACE water storage and estimated baseflow data, Water Resour. Res., accepted, 2009. 4817

Milly, P. C. and Shmakin, A. B.: Global modeling of land water and energy balances. Part I: The Land Dynamics (LaD) model, J. Hydrometeorol., 3, 283–299, 2002. 4815

Nash, J. E. and Sutcliffe, J. V.: River flow forecasting through conceptual models part 1 – A discussion of principles, J. Hydrol., 10, 282–290, 1970. 4822

Ngo-Duc, T., Laval, K., Ramillien, G., Polcher, J., and Cazenave, A.: Validation of the land water storage simulated by Organising Carbon and Hydrology in Dynamic Ecosystems (ORCHIDEE) with Gravity Recovery and Climate Experiment (GRACE) data, Water Resour. Res., 43, W04427, doi:doi:10.1029/2006WR004941, 2007. 4816, 4817

Niu, G.-Y., Yang, Z.-L., Dickinson, R. E., Gulden, L. E., and Su, H.: Development of a simple groundwater model for use in climate models and evaluation with Gravity Recovery and Climate Experiment data, J. Geophys. Res., 112, D07103, doi:10.1029/2006JD007522, 2007. 4815, 4817

Papa, F., Güntner, A., Frappart, F., Prigent, C., and Rossow, W. B.: Variations of surface water extent and water storage in large river basins: A comparison of different global data sources, Geophys. Res. Lett., 35, L11401, doi:10.1029/2008GL033857, 2008. 4817, 4818, 4830, 4839

Parajka, J. and Blöschl, G.: The value of MODIS snow cover data in validating and calibrating conceptual hydrologic models, J. Hydrol., 358, 240-258, doi:10.1016/j.jhydrol.2008.06.006, 2008. 4839

Peel, M. C., Finlayson, B. L., and McMahon, T. A.: Updated world map of the Kppen-Geiger climate classification, Hydrol. Earth Syst. Sci., 11, 1633–1644, 2007,

Title Page

Abstract | Introduction

Conclusions | References

Tables | Figures

|◄ | ►|

◄ | ►

Back | Close

Full Screen / Esc

Printer-friendly Version

Interactive Discussion

http://www.hydrol-earth-syst-sci.net/11/1633/2007/. 4852

Priestley, C. H. and Taylor, R. J.: On the assessment of surface heat flux and evaporation using large-scale parameters, Mon. Weather Rev., 100, 81–92, 1972. 4820

Reichle, R. H., McLaughlin, D. B., and Entekhabi, D.: Hydrologic Data Assimilation with the Ensemble Kalman Filter, Mon. Weather Rev., 130, 103–114, 2002. 4816

Rodell, M., Houser, P. R., Jambor, U., Gottschalck, J., Mitchell, K., Meng, C. J., Arsenault, K., Cosgrove, B., Radakovich, J., Bosilovich, J. K. E. M., Walker, J. P., Lohmann, D., and Toll, D.: The Global Land Data Assimilation System, B. Am. Meteorol. Soc., 85, 381–394, 2004. 4815

Rodell, M., Chen, J., Kato, H., Famiglietti, J., Nigro, J., and Wilson, C.: Estimating groundwater storage changes in the Mississippi River basin (USA) using GRACE, Hydrogeol. J., 15, 159–166, 2007. 4831

Savenije, H. H. G.: *HESS Opinions* "The art of hydrology", Hydrol. Earth Syst. Sci., 13, 157–161, 2009,

http://www.hydrol-earth-syst-sci.net/13/157/2009/. 4816

Schmidt, R., Schwintzer, P., Flechtner, F., Reigber, C., Güntner, A., Döll, P., Ramillien, G., Cazenave, A., Petrovic, S., Jochmann, H., and Wünsch, J.: GRACE observations of changes in continental water storage, Global Planet. Change, 50, 112–126, 2006. 4816, 4818

Schmidt, R., Flechtner, F., Meyer, U., Neumayer, K. H., Dahle, C., König, R., and Kusche, J.: Hydrological signals observed by the GRACE satellites, Surv. Geophys., 29, 319–334, 2008a. 4817, 4825, 4826

Schmidt, R., Petrovic, S., Güntner, A., Barthelmes, F., Wünsch, J., and Kusche, J.: Periodic components of water storage changes from GRACE and global hydrology models, J. Geophys. Res., 29, 319-334, 2008b. 4816, 4818

Schulze, K. and Döll, P.: Neue Ansätze zur Modellierung von Schneeakkumulation und -schmelze im globalen Wassermodell WaterGAP, in: 7th Workshop for large-scale modeling in Hydrology. Munic, November 2003, edited by Ludwig, R., Reichert, D., and Mauser, W., 145–154, Kassel University Press, Kassel, 2004. 4816

Seitz, F., Schmidt, M., and Shum, C. K.: Signals of extreme weather conditions in Central Europe in GRACE 4-D hydrological mass variations, Earth Planet. Sc. Lett., 268, 165–170, 2008. 4817, 4832

Sheffield, J., Ferguson, C. R., Troy, T. J., Wood, E. F., and McCabe, M. F.: Closing the terrestrial water budget from satellite remote sensing, Geophys. Res. Lett., 36, L07403,

doi:10.1029/2009GL037338, 2009. 4817

Shuttleworth, W. J.: Evaporation, in: Handbook of hydrology, edited by: Maidment, D., 4.1–4.53, McGraw-Hill Inc., 1993. 4820

Swenson, S. and Wahr, J.: Methods for inferring regional surface-mass anomalies from Gravity Recovery and Climate Experiment (GRACE) measurements of time-variable gravity, J. Geophys. Res., 107, 2193, doi:10.1029/2001JB000576, 2002. 4817, 4825, 4847

Swenson, S., Famiglietti, J., Basara, J., and Wahr, J.: Estimating profile soil moisture and groundwater variations using GRACE and Oklahoma Mesonet soil moisture data, Water Resourses Research, 44, W01413, doi:10.1029/2007WR006057, 2008. 4817

Syed, T. H., J. S., F., Rodell, M., Chen, J., and Wilson, C. R.: Analysis of terrestrial water storage changes from GRACE and GLDAS, Water Resourses Research, 44, W02433, doi:10.1029/2006WR005779, 2008. 4815, 4817

Tang, Y., Reed, P., and Wagener, T.: How effective and efficient are multiobjective evolutionary algorithms at hydrologic model calibration?, Hydrol. Earth Syst. Sc., 10, 289–307, 2006. 4823

Tapley, B. D., Bettadpur, S., Watkins, M., and Reigber, C.: The gravity recovery and climate experiment: Mission overview and early results, Geophys. Res. Lett., 31, L09607, doi:10.1029/2004GL019920, 2004. 4816

Vrugt, J. A., Gupta, H. V., Bastidas, L. A., Bouten, W., and Sorooshian, S.: Effective and efficient algorithm for multiobjective optimization of hydrologic models, Water Resour. Res., 39, 1214, doi:10.1029/2002WR001746, 2003. 4817, 4823

Wahr, J., Swenson, S., Zlotnicki, V., and Velicogna, I.: Time-variable gravity from GRACE: First results, Geophys. Res. Lett., 31, L11501, doi:10.1029/2004GL019779, 2004. 4816

Wahr, J., Swenson, S., and Velicogna, I.: Accuracy of GRACE mass estimates, Geophys. Res. Lett., 33, L06401, doi:10.1029/2005GL025305, 2006. 4826

Werth, S., Güntner, A., Petrovic, S., and Schmidt, R.: Integration of GRACE mass variations into a global hydrological model, Earth Planet. Sc. Lett., 277, 166–173, 2009a. 4817, 4821, 4822, 4823

Werth, S., Güntner, A., Schmidt, R., and Kusche, J.: Evaluation of GRACE filter tools from a hydrological perspective, Geophys. J. Int., in review, 2009b. 4815, 4817, 4825, 4853

Widen-Nilsson, E., Halldin, S., and Xu, C.-y.: Global water-balance modelling with WASMOD-M: Parameter estimation and regionalisation, J. Hydrol., 340, 105–118, 2007. 4815

Winsemius, H. C., Savenije, H. H. G., Gerrits, A. M. J., Zapreeva, E. A., and Klees, R.: Com-

parison of two model approaches in the Zambezi river basin with regard to model reliability and identifiability, Hydrol. Earth Syst. Sci., 10, 339–352, 2006a, http://www.hydrol-earth-syst-sci.net/10/339/2006/. 4833

Winsemius, H. C., Savenije, H. H. G., van de Giesen, N. C., van den Hurk, B. J. J. M., Za-preeva, E. A., and Klees, R.: Assessment of Gravity Recovery and Climate Experiment (GRACE) temporal signature over the upper Zambezi, Water Resour. Res., 42, W12201, doi:10.1029/2006WR005192, 2006b. 4838

Wouters, B., Chambers, D., and Schrama, E. J.: GRACE observes small-scale mass loss in Greenland, Geophys. Res. Lett., 35, L20501, doi:10.1029/2008GL034816, 2008. 4817

Yapo, P. O., Gupta, H. V., and Sorooshian, S.: Mulit-objective global optimization for hydrologic models, J. Hydrol., 204, 83–97, 1998. 4817

Zaitchik, B. F., Rodell, M., and Reichle, R. H.: Assimilation of GRACE terrestrial water storage data into a land surface model: Results for the Mississippi River Basin, J. Hydrometeorol., 9, 535–548, 2008. 4817, 4831

Zeng, N., Yoon, J.-H., Marengo, J. A., Subramaniam, A., Nobre, C. A., Mariotti, A., and Neelin, J. D.: Causes and impacts of the 2005 Amazon drought, Environ. Res. Lett., 3, 014002, doi:10.1088/1748-9326/3/1/014002, 2008. 4817, 4830

Title Page

Abstract | Introduction

Conclusions | References

Tables | Figures

|◄ | ►|

◄ | ►

Back | Close

Full Screen / Esc

Printer-friendly Version

Interactive Discussion

Table 1. Detail information on the calibration parameter (col. 1; MCWH: maximum canopy water height, MPET: maximum potential evapotranspiration, PT: Priestley-Taylor) is provided by belonging processes and numbering (col. 2; SL: Soil, GW: groundwater, SW: Surface water, ER: Evaporation and Radiation, SN: Snow, IN: Interception), original WGHM value (col. 3), minimum and maximum value (col. 4,5). Literature references to model parameter and according equation numbers are provided in columns 6 and 7, English references are preferred.

Parameter	Abbrev. number	Original value and unit	Min. value	Max. value	Literature reference	(Eq.) or page
Root depth mult.	SL-1	1	0.5	2	Kaspar (2004)	(2.26)
GW baseflow coefficient	GW-1	0.01/day	0.006	0.1	Döll et al. (2003)	(5)
Runoff coefficient mult.	SW-1	1	0.5	2	Döll et al. (2003)	(3)
River velocity	SW-2	1 m/s	0.05	2	Kaspar (2004)	(2.38)
Lake depth	SW-3	5 m	1	20	Döll et al. (2003)	(6)
Wetland depth	SW-4	2 m	1	5	Döll et al. (2003)	(6)
SW baseflow coefficient	SW-5	0.01/day	0.001	0.1	Döll et al. (2003)	(6)
Radiation proportion	ER-1	0.25	0.08	0.54	Kaspar (2004)	(2.11)
Radiation correction	ER-2	1.0	0.7	1.3	Kaspar (2004)	(2.13)
Albedo snow	ER-3	0.4	0.3	0.9	Kaspar (2004)	p. 19
Albedo oben water	ER-4	0.08	0.03	0.5	Kaspar (2004)	p. 15
PT coeff. (humid areas)	ER-5	1.26	0.885	1.65	Kaspar (2004)	(2.4)
PT coeff. (arid areas)	ER-6	1.74	1.365	2.115	Kaspar (2004)	(2.4)
MPET	ER-7	10 mm/day	6.25	13.75	Döll et al. (2003)	(2)
MCWH	IN-1	0.3 mm	0.1	1.4	Döll et al. (2003)	(1)
Specific leaf area mult.	IN-2	1	−0.2	2.2	Kaspar (2004)	(2.19)
Biomass mult.	IN-3	1	0.25	1.75	Kaspar (2004)	(2.19)
Snow freeze temperature	SN-1	0°C	−1	3	Kaspar (2004)	(2.22)
Snow melt temperature	SN-2	0°C	−3.75	3.75	Güntner et al. (2007)	(2)
Degree day factor	SN-3	1	0.5	2	Güntner et al. (2007)	(2)
Temperature gradient	SN-4	0.006°C/m	0.004	0.01	Hunger and Döll (2008)	p. 845

Table 2. Details of the 28 calibrated river basins (col. 1–3) and calibration data (col. 4–6) used. Col. 4: River runoff station, col. 5: Source of discharge data (1: GRDC, 2: US-ACE, 3: ORE-HYBAM) and period runoff data applied for calibration, col. 7: applied GRACE filter method and belonging filter parameter (I: isotropic filter of Swenson and Wahr (2002) for an a-priori given maximum error of basin average Δ_{max}; II: Swenson and Wahr (2002) computed by by the auto-correlation length G_l and standard deviation σ_0 of an exponential signal model; III: decorelation method by Kusche (2007) with the power x of the regularization factor $a=10^x$ of the signal covariance matrix).

No.	Basin	Basin area [Mio km^2]	Discharge data source & period	Discharge station	Filter parameter (I) a (II) Δ_{max}, (III) σ_0/G_l	
B1	Amazon	5.96	3: 2003-2007	Obidos	III:	250/300
B2	Amur	1.87	1: 1975–2004	Bogorodskoye	II:	2.5
B3	Columbia	0.67	1: 1977–2006	Dalles	I:	13
B4	Danube	0.80	1: 1973–2002	Ceatal Izmail	I:	12
B5	Ganges	1.59	1: 1973–2002	Farakka	I:	12
B6	Huang He	0.80	1: 1973–2002	Huayuankou	I:	13
B7	Indus	0.85	1: 1950–1979	Kotri	III:	200/1000
B8	Lena	2.45	1: 1973–2002	Stolb	I:	12
B9	Mackenzie	1.70	2: 2003–2007	Arctic Red River	III:	150/200
B10	Mekong	0.80	1: 1980–1991	Kompong Cham	I:	12
B11	Mississippi	3.24	1: 2003–2007	Tarbert Landing	I:	12
B12	Murray	1.06	1: 1965–1984	Lock 9	III:	150/900
B13	Nelson	1.20	1: 1976–2005	Kelsey	I:	12
B14	Niger	1.80	1: 1977–2006	Lokoja	I:	12
B15	Nile	2.91	1: 1973–1984	El Ekhsase	III:	150/900
B16	Ob	2.70	2: 2003–2007	Salekhard	I:	13
B17	Orange	0.96	1: 1972–2001	Vioolsdrif	III:	20/1000
B18	Orinoco	0.97	1: 1960–1989	Tunene Angostura	II:	4.1
B19	Parana	2.58	1: 1965–1994	Timbues	I:	12
B20	St. Lawrence	1.05	1: 1976–2005	Cornwall	III:	200/1000
B21	Tocantins	0.88	1: 1978–1999	Tucurui	I:	12
B22	Volga	1.39	1: 1973–2002	Volgograd	I:	13
B23	Volta	0.41	1: 1955–1984	Senchi	I:	13
B24	Yangtze	1.93	1: 1975–2004	Datong	I:	12
B25	Yenisei	2.54	2: 2003–2007	Igarka	I:	14
B26	Yukon	0.83	1: 1977–2006	Pilot Stn.	III:	150/100
B27	Congo (Zaire)	3.72	1: 1954–1983	Kinshasa	I:	13
B28	Zambezi	1.39	1: 1976–1979	Matundo-Cais	I:	12

Title Page

Abstract | Introduction

Conclusions | References

Tables | Figures

|◄ | ►|

◄ | ►

Back | Close

Full Screen / Esc

Printer-friendly Version

Interactive Discussion

Table 3. Most sensitive calibrated parameter for the 28 river basins. See Table 2 for complete basin names and parameter description.

B1	B2	B3	B4	B5	B6	B7	B8	B9	B10
SL-1	SL-1	SL-1	SL-1	SL-1	SW-1	SW-1	SL-1	SW-1	SL-1
GW-1	SW-1	SW-1	SW-1	GW-1	SW-5	SW-2	SW-1	SW-3	GW-1
SW-1	ER-3	ER-1	SW-3	SW-3	ER-3	SW-5	ER-1	SW-5	SW-1
SW-2	ER-1	ER-3	ER-1	SW-4	IN-1	ER-1	ER-3	ER-3	SW-2
SW-4	IN-1	SN-2	ER-5	ER-1	IN-2	ER-3	ER-5	ER-4	SW-4
IN-1	SN-2	SN-4	SN-2	SN-2	IN-3	ER-5	IN-1	SN-1	IN-1
						SN-2	IN-2	SN-2	IN-2
						SN-4	SN-2	SN-3	IN-3

B11	B12	B13	PB14	B15	B16	B17	B18	B19	B20
SL-1	GW-1	SW-1	SL-1	SL-1	SW-1	GW-1	SL-1	SL-1	SL-1
SW-1	SW-1	SW-5	GW-1	GW-1	SW-2	SW-1	GW-1	GW-1	SW-1
ER-1	SW-5	ER-1	SW-2	SW-2	SW-5	ER-7	SW-2	SW-1	SW-3
ER-5	ER-2	ER-3	SW-4	SW-3	ER-2	IN-1	SW-5	SW-3	ER-4
IN-1	ER-5	ER-4	SW-3	SW-4	ER-3	IN-2	ER-1	SW-4	ER-5
SN-2	ER-6	ER-5	ER-1	ER-1	SN-1	IN-3	IN-2	SW-5	IN-1
	IN-1	SN-2	IN-2	ER-3	SN-2			ER-1	IN-2
	IN-2	SN-3	IN-1	SN-2	SN-3			ER-5	SN-2

B21	B22	B23	B24	B25	B26	B27	B28
SL-1	SL-1	SL-1	SL-1	ER-1	SL-1	SL-1	SL-1
GW-1	GW-1	GW-1	SW-2	ER-3	SW-1	GW-1	ER-6
SW-2	SW-2	SW-1	ER-1	ER-5	SW-4	SW-4	SW-1
SW-3	SW-3	SW-2	ER-3	SN-1	ER-1	SW-5	SW-3
SW-4	ER-1	SW-3	ER-5	SN-2	ER-3	ER-1	ER-1
ER-1	SN-2	ER-1	SN-2	SN-3	SN-2	ER-5	ER-7
ER-4		IN-1					IN-1
IN-2		IN-2					IN-2

Table 4. Root mean squared signal of observed river discharge ($\sigma_{\mathrm{Dis}}^{\mathrm{meas}}$, col. 2) and standard deviation of GRACE TWSV ($\sigma_{\mathrm{TWSV}}^{\mathrm{meas}}$, col. 5) compared to the root mean squared error (RMSE) of the calibrated (ϵ^{cal}, col. 3 and 6) and the original (ϵ^{org}, col. 4 and 7) model against respective observation data for all 28 river basins. Col. 8 provides differences of RMSE values of TWSV from the calibrated and the original model for the validation period (01/2008–12/2008). Here, negative values indicate an improved simulation compared of the calibrated compared to the original model.

Basin No.	$\sigma_{\mathrm{Dis}}^{\mathrm{meas}}$ [km³/mth]	$\epsilon_{\mathrm{Dis}}^{\mathrm{cal}}$ [km³/mth]	$\epsilon_{\mathrm{Dis}}^{\mathrm{org}}$ [km³/mth]	$\sigma_{\mathrm{TWSV}}^{\mathrm{meas}}$ [mm]	$\epsilon_{\mathrm{TWSV}}^{\mathrm{cal}}$ [mm]	$\epsilon_{\mathrm{TWSV}}^{\mathrm{org}}$ [mm]	$\Delta\epsilon_{\mathrm{TWSV}}^{2008}$(cal−org) [mm]
B1	471	39	149	118	29	53	−31
B2	31	10	11	30	25	29	−2
B3	13	4	6	65	33	35	−3
B4	17	2	6	61	28	36	−7
B5	44	9	19	103	21	24	2
B6	4	2	2	26	25	26	0.4
B7	11	3	3	40	26	28	2
B8	64	14	24	31	16	20	−10
B9	29	9	14	34	15	20	−10
B10	34	6	3	113	42	54	−14
B11	42	5	15	41	18	26	−12
B12	0.8	0.4	0.8	24	15	16	−0.1
B13	5.3	0.3	2	46	20	20	−1
B14	18	2	16	76	23	29	−5
B15	3	1	17	50	22	27	−6
B16	43	15	21	46	20	23	−5
B17	0.7	0.3	0.6	12	9	9	−0.1
B18	98	20	31	168	36	50	18
B19	45	4	33	49	17	20	−7

Table 4. Continued.

Basin No.	σ_{Dis}^{meas} [km³/mth]	ϵ_{Dis}^{cal} [km³/mth]	ϵ_{Dis}^{org} [km³/mth]	σ_{TWSV}^{meas} [mm]	ϵ_{TWSV}^{cal} [mm]	ϵ_{TWSV}^{org} [mm]	$\Delta\epsilon_{TWSV}^{2008}$(cal−org) [mm]
B20	20	1	2	39	38	50	−19
B21	36	4	14	157	36	46	−10
B22	23	2	20	48	22	35	−7
B23	3	0.9	1	84	38	42	−7
B24	80	10	18	36	17	19	−3
B25	73	23	38	37	16	16	−0.4
B26	21	8	10	65	20	20	−5
B27	112	9	25	41	25	24	−4
B28	9	2	5	107	52	67	−25

Table 5. Variability of unfiltered and basin-averaged continental TWSV simulations from the calibrated WGHM version for total storage and single compartments: σ^{cal}(storage) (TS: total storage, SL: soil, GW: groundwater, SN: snow, R: river, SW: surface water, C: canopy). Every other line provides deviations of storage variability to the original model: $\Delta\sigma_{storage}=\sigma^{cal}$(storage)$-\sigma^{org}$(storage).

Basin	$\sigma^{cal}(TS)$	$\Delta\sigma_{TS}$	$\sigma^{cal}(SL)$	$\Delta\sigma_{SL}$	$\sigma^{cal}(GW)$	$\Delta\sigma_{GW}$	$\sigma^{cal}(SN)$	$\Delta\sigma_{SN}$	$\sigma^{cal}(R)$	$\Delta\sigma_{R}$	$\sigma^{cal}(SW)$	$\Delta\sigma_{SW}$	$\sigma^{cal}(C)$	$\Delta\sigma_{C}$
B1	150	+60	37	+8	25.7	+0.4	0.1	+0.0	82.9	+49.6	2.1	+0.8	0.0	+0.0
B2	20	+3	10	+3	7.8	−0.4	21.0	+1.7	5.0	+0.2	1.4	+0.2	0.5	+0.3
B3	55	-1	12	−7	4.4	−0.6	40.2	+6.1	3.5	+0.1	1.7	−0.2	0.2	+0.0
B4	64	+4	43	13	10.6	−2.2	16.0	−9.4	4.1	−3.0	1.4	+0.9	0.4	+0.0
B5	90	+7	17	−8	21.0	−5.6	1.8	+0.3	20.1	+3.6	10.6	+4.2	0.1	+0.1
B6	18	-2	9	+1	5.9	−1.4	0.3	+0.0	2.7	−0.6	0.3	−0.2	0.1	+0.1
B7	28	+4	7	+1	4.8	+0.7	24.6	+3.4	6.4	+0.2	1.0	+0.4	0.0	+0.0
B8	32	+0	8	+2	1.7	+0.2	47.9	+2.8	15.2	+4.7	1.8	+0.1	0.8	+0.5
B9	44	-8	7	−1	7.8	+0.5	50.7	+0.1	6.9	+3.5	1.5	−1.3	0.3	+0.0
B10	129	+36	54	+22	33.5	+0.6	0.3	+0.0	37.1	+11.2	3.1	+0.7	0.1	+0.1
B11	48	+14	27	+11	6.3	−0.4	12.1	+2.6	3.4	−0.6	1.9	+0.0	1.1	+0.9
B12	17	+3	9	+1	2.1	−0.6	0.0	+0.0	0.6	+0.4	2.4	+0.7	0.0	−0.1
B13	57	+2	10	−1	12.2	+1.2	39.8	+2.4	0.5	−0.2	7.7	+0.5	0.2	+0.0
B14	58	+14	26	+12	14.8	−4.6	0.0	+0.0	11.1	+4.2	3.2	−0.2	2.6	+2.6
B15	35	+2	21	+8	1.6	−5.3	0.0	+0.0	9.7	+1.2	3.5	+0.3	0.0	+0.0
B16	61	+0	14	−2	14.6	+2.2	67.5	+9.3	5.3	+0.4	1.5	−0.7	0.3	+0.0
B17	6	−1	3	−1	2.3	−0.3	0.0	+0.0	0.5	−0.3	0.4	−0.1	0.3	+0.3
B18	169	+51	57	+18	35.8	+1.7	0.0	+0.0	54.6	+26.0	7.6	+1.3	0.1	+0.0
B19	59	+1	22	+6	19.3	−0.8	0.0	+0.0	5.1	−10.3	5.6	+2.4	0.1	+0.0
B20	78	−20	15	−5	9.8	−4.9	43.4	−21.4	1.2	−1.4	9.2	−0.3	0.6	+0.3
B21	145	+18	39	+17	43.0	+0.8	0.0	+0.0	16.0	−9.4	13.1	+2.3	0.3	+0.3
B22	68	−16	33	+8	11.9	−2.6	56.0	−15.1	11.5	−5.4	1.7	+0.6	0.3	+0.0
B23	80	+26	49	+28	19.2	+1.9	0.0	+0.0	2.5	−0.4	4.6	−1.8	1.0	+1.0
B24	30	−5	4	−2	13.0	+1.2	1.2	+0.5	12.3	−3.4	0.7	+0.0	0.3	+0.0
B25	41	+2	9	+1	6.8	+1.3	56.0	+7.5	9.1	+3.9	1.9	+0.5	0.3	+0.0
B26	52	−3	7	+0	3.4	+0.3	57.6	+0.0	8.8	+1.1	2.9	+0.5	0.2	+0.0
B27	47	+9	26	+12	6.3	−8.8	0.0	+0.0	7.3	+1.2	2.8	+0.6	0.0	+0.0
B28	80	+26	41	+20	23.3	+5.3	0.0	+0.0	3.6	−0.7	9.1	+2.6	0.0	+0.0
global	66	+7	24	+3	15.4	−0.6	20.5	+0.2	9.4	+3.3	13.2	+2.7	0.2	+0.1

Title Page

Abstract | Introduction

Conclusions | References

Tables | Figures

◀ | ▶

◀ | ▶

Back | Close

Full Screen / Esc

Printer-friendly Version

Interactive Discussion

Fig. 1. The 28 largest and most important river basins worldwide (black polygons) with under-lying Köppen-Geiger climate zones (for 1951–2000, by Peel et al., 2007) and gauging stations (white diamonds) of each basin used for calibration of river discharge. See Table 2 for station names.
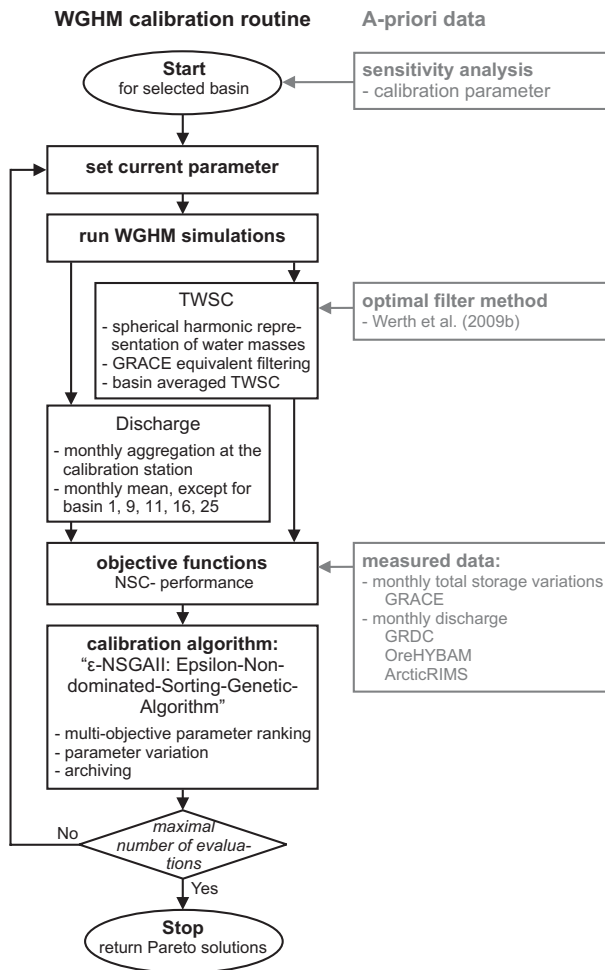
Fig. 2. Concept scheme of multi-objective WGHM calibration for a specific river basin and with input from Werth et al. (2009b) for applied GRACE filter methods.
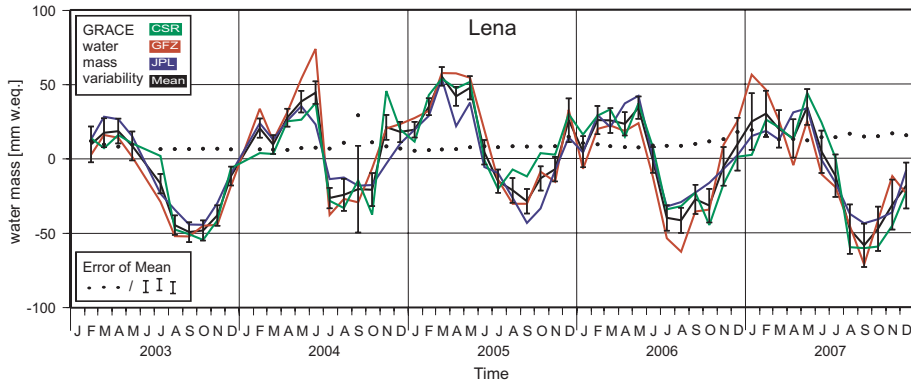
Fig. 3. Basin-averaged time series of TWS variations from GRACE for the Lena river basin from the processing centres CSR (green), GFZ (red) and JPL (blue) and the averaged field (black) with propagated coefficient errors (black dots and error bars).
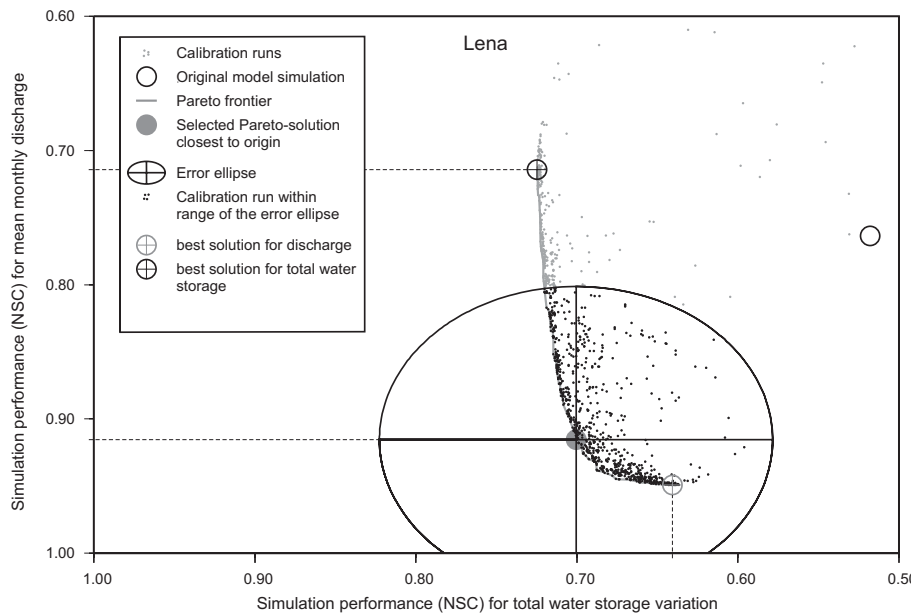
Fig. 4. Calibration results for the Lena river basin in terms of objective function values. Each point (gray and black) represents one model run. The Pareto optimal solutions form a frontier (gray solid line) towards the optimal model fit (lower left corner). The Pareto solution closest to the optimum (gray large dot) is selected as the optimal solution of the calibration providing a balanced improvement for both objectives and it is used for further studies. Best solutions for each single objective are located at the end of the Pareto frontier (crossed large dots). From errors of the measured calibration data, an uncertainty range for both objectives is indicated by an error ellipse around the selected Pareto solution. The solutions lying in that range (black small dots) show a significant improvement of the calibrated model compared to the original model simulation (plain black circle).
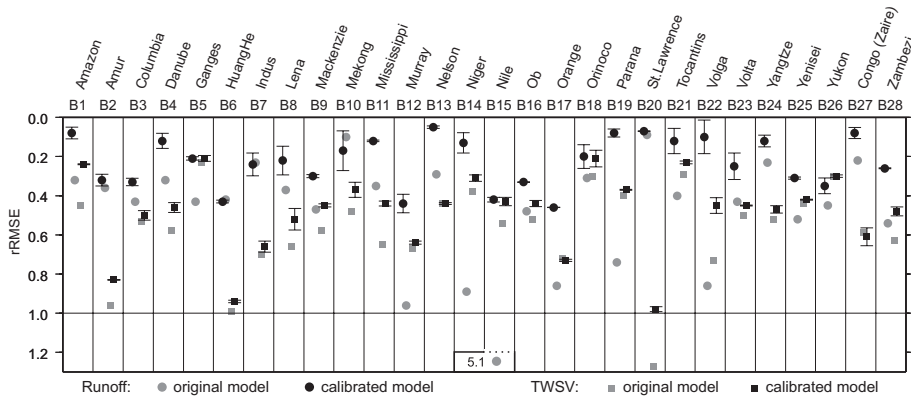
Fig. 5. Simulation performance for the 28 calibrated river basins in terms of relative root mean squared error (rRMSE) for river discharge (circles) and TWSV (squares) of the original (gray) and the calibrated model version (black). See Table 4 for absolute values. Error bars are derived from GRACE and discharge measurement errors as described in Sect. 2.4.
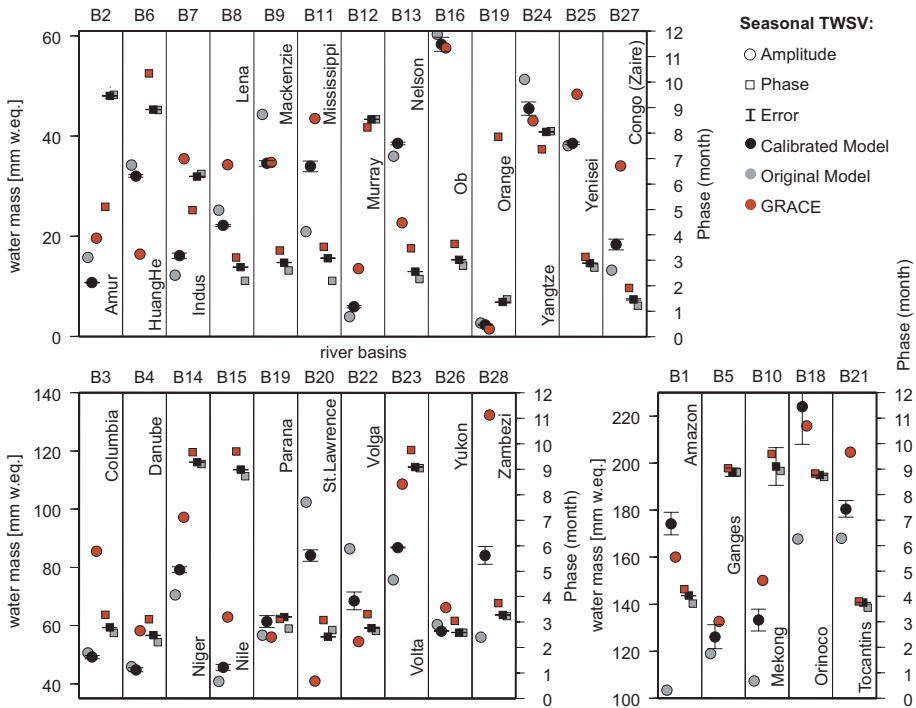
Fig. 6. Results for seasonal amplitude (circles) and phase (squares) of TWSV for the original (gray) and the calibrated model version (black) compared to GRACE (red). Error bars of TWSV amplitudes are derived from GRACE and discharge measurement errors as described in Sect. 2.4.
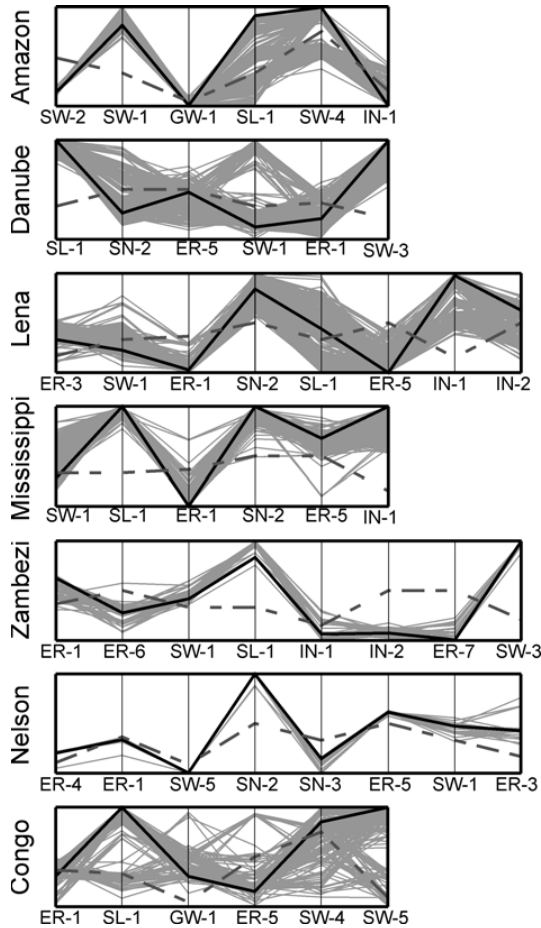
Fig. 7. Normalized parameter for exemplary river basins. Parameter sets are shown for the selected optimum (black solid line), the original model version (gray dashed line) and all calibration runs within the uncertainty range (gray solid lines) due to observational errors.
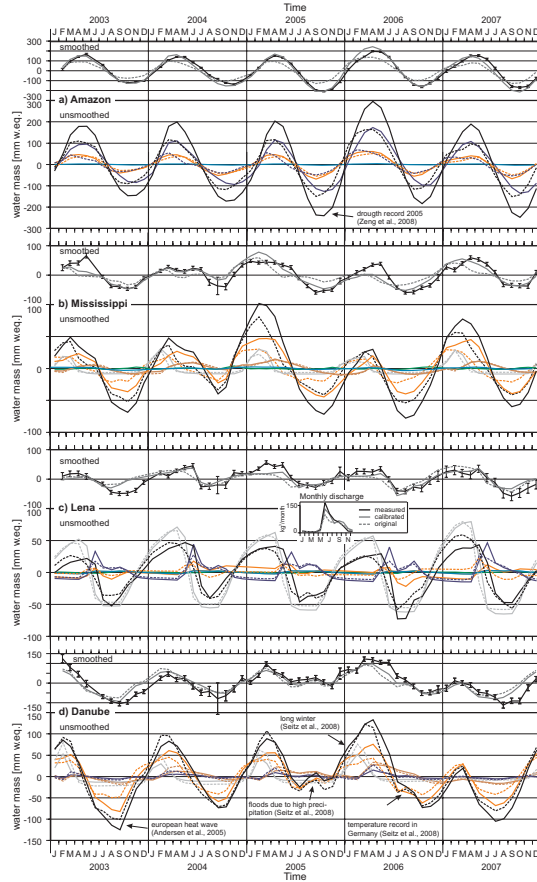
Fig. 8. Basin-averaged time series of single storage compartments from the calibrated and the original model version (unsmoothed, below) as well as smoothed total storage from both model versions and GRACE (smoothed, above) for **(a)** the Amazon, **(b)** the Mississippi, **(c)** the Lena and **(d)** the Danube basin. See Fig. 9 for legend.
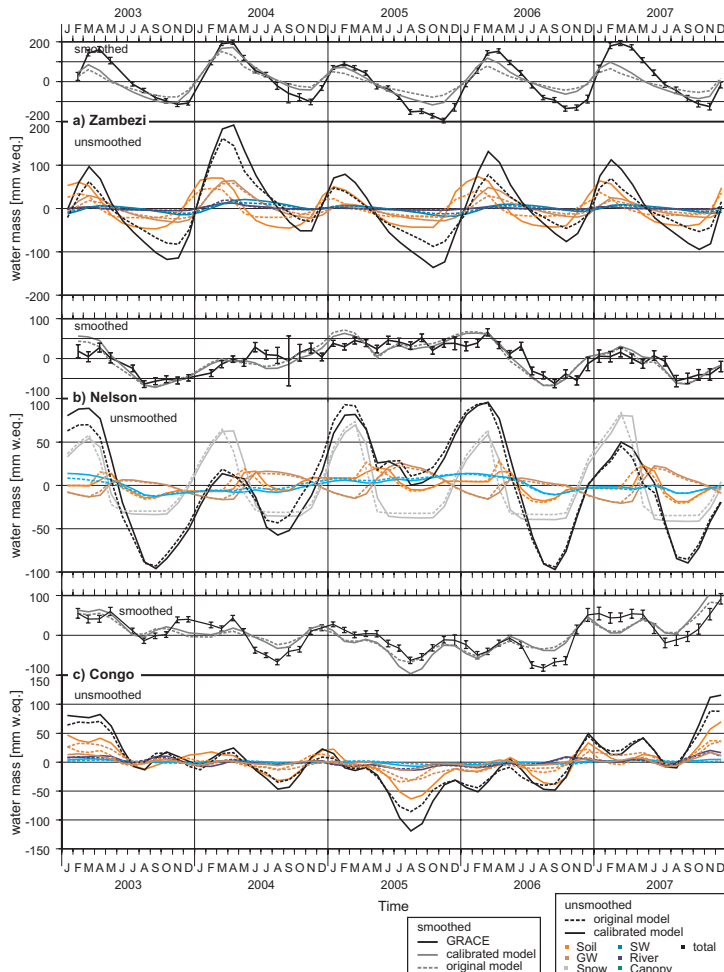
Fig. 9. Same as Fig. 8 but for **(a)** the Zambezi, **(b)** the Nelson and **(c)** the Congo basin.
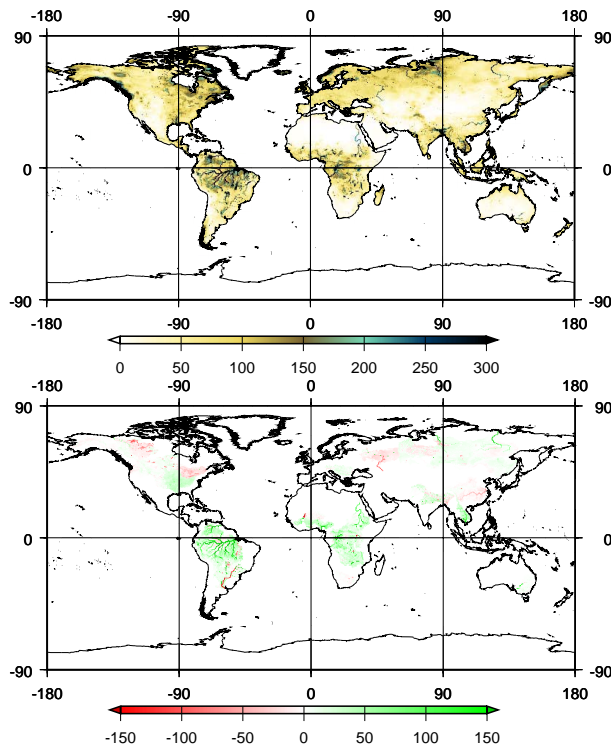
Fig. 10. Global distribution of total storage variability of the calibrated WGHM (above) and its deviations to the original model version (below). Negative values below indicate decreased and positive values increased variability. Units are in mm of water column.